Hepatitis B Virus Protein pX Enhances the Monomer Assembly Pathway of bZIP·DNA Complexes[†]

Tanya L. Schneider and Alanna Schepartz*

Department of Chemistry, Yale University, New Haven, Connecticut 06511

Received October 23, 2000; Revised Manuscript Received December 18, 2000

ABSTRACT: The rapid and correct assembly of dimeric transcription factors on target DNA is essential for accurate transcriptional regulation. Here we ask how a viral accessory factor, hepatitis B virus X protein (pX), influences the rate and identity of the assembly pathway followed by members of the basic region leucine zipper (bZIP) transcription factor family. A combination of fluorescence polarization and fluorescence resonance energy transfer (FRET) experiments demonstrates unequivocally that pX does not increase the concentration of properly folded bZIP dimers in solution. Rather, fluorescence polarization and gel mobility shift experiments reveal that pX interacts directly with the basic-spacer segment of the bZIP peptide and stabilizes the complex composed of this monomer and target DNA. By stabilizing the intermediate formed along the monomer assembly pathway but not the one formed along the dimer pathway, pX enhances the equilibrium stability of a bZIP·DNA complex without changing the molecular mechanism used for complexation. Additional experiments reveal that pX decreases the kinetic specificity of certain bZIP proteins. To the extent that it is reflected at the transcriptional level, this loss in specificity could have far-reaching consequences for the host cell.

The hepatitis B virus (HBV)[1] has infected more than 2 billion members of the current population, and more than 350 million individuals are infected chronically (*1*). Studies show a clear connection between chronic HBV infection and the development of hepatocellular carcinoma (HCC) and suggest that chronic infection confers a 100-fold greater risk of developing HCC (*1−4*). The HBV genome encodes at least seven proteins, including structural viral envelope and core proteins, a DNA polymerase, and the 16.5 kDa X protein (pX) (*5*). Though pX is not homologous to any known nonviral protein sequence, it is conserved among most Hepadnaviridae (*6, 7*). pX is implicated in HBV pathogenesis as it is necessary for viral infection (*8−10*) and contributes to the malignant transformation of fetal mouse cells (*11*). Other studies note the development of HCC in transgenic mice engineered to express pX (*12, 13*), and pX has been linked to the development of liver cancer after HBV infection (*14−16*). A precise understanding of the molecular basis of pX activity is critical because of its direct role in the development of HCC.

pX is present and active in both the cytoplasm and the nucleus of virally infected host cells (*7, 17−20*). In the cytoplasm, a myriad of roles for pX has been proposed, including stimulation of signal transduction cascades (*21−*

25), inactivation of p53 function (*26*), and induction of apoptosis with (*27*) or without (*28−30*) p53 involvement. In the nucleus, pX enhances transcription from a variety of DNA target sites (*31−35*), though it does not itself possess high intrinsic DNA affinity (*36, 37*). pX has also been shown to interact directly with basal transcription factors (*38−40*) as well as basic region leucine zipper (bZIP) transcription factors (*41, 42*) to promote transcription (*14, 36, 43−45*).

The interactions of pX with bZIP transcription factors in the CREB-ATF subfamily (*41, 42*) serve to increase the affinity of these proteins for target DNA (*45−47*). pX also alters the DNA specificities of these proteins, selectively enhancing their affinity for the HBV enhancer element (*36*). Work with bZIP peptides identified the bZIP element (*48*), the 60-amino acid DNA binding domain, of CREB and ATF-2 as the primary site of interaction with pX (*45−47*). Several studies have provided an initial look at how pX might interact with bZIP proteins to increase their affinity for DNA. All studies agree that pX interacts with the bZIP element to increase DNA affinity. One study indicates that this interaction increases the stability of the bZIP dimer as well as the affinity of the dimer for DNA (*46*). Another study suggests that this pX−bZIP interaction promotes dimerization in the absence of DNA, thereby leading to an increased level of DNA binding (*47*).

In the absence of pX, a bZIP protein binds target DNA to yield a 2:1 bZIP·DNA complex. Recent data suggest that, for all bZIP proteins that have been examined, the pathway by which this ternary complex assembles is one in which two bZIP monomers bind DNA sequentially and subsequently assemble their dimerization interface while bound to DNA (*49−53*). The other potential pathway, in which two monomers dimerize first and then bind DNA, is not feasible

* To whom correspondence should be addressed. Phone: (203) 432-5094. Fax: (203) 432-3486. E-mail: alanna.schepartz@yale.edu.

[1] Abbreviations: HBV, hepatitis B virus; HCC, hepatocellular carcinoma; bZIP, basic region leucine zipper; CRE, cyclic AMP response element; ESMS, electrospray mass spectrometry; FRET, fluorescence resonance energy transfer; HTLV-I, human T-cell leukemia virus type I.
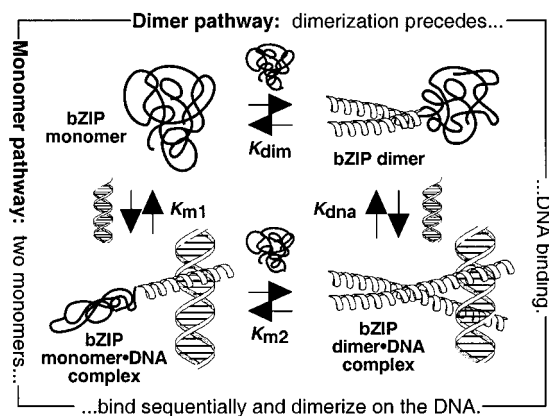
FIGURE 1: Two limiting pathways for assembly of bZIP·DNA complexes.

due to the limiting rate of bZIP dimerization. The two assembly pathways are outlined in Figure 1. Here we ask how the assembly of a bZIP·DNA complex is impacted by pX, given the significant effect of pX on bZIP·DNA complex stability. In particular, we ask whether pX enhances one or more steps along the existing monomer pathway, or whether it enhances dimerization to the extent that the dimer pathway competes effectively. Previous studies investigating the effect of pX on the bZIP monomer–dimer equilibrium have provided conflicting descriptions of the relationship between pX and the concentration of bZIP dimers in solution in the absence of DNA (*45*, *47*).

In this work, we use a combination of fluorescence and gel mobility shift experiments to investigate the effect of pX on bZIP dimerization and the mechanism of bZIP·DNA complexation. Initial fluorescence polarization experiments confirmed that pX interacts directly with bZIP peptides. Fluorescence resonance energy transfer (FRET) studies of bZIP dimer formation, however, revealed that this interaction has no effect on the concentration of bZIP dimers in solution. Subsequent fluorescence polarization experiments demonstrated that pX interacts directly with the basic-spacer region of a bZIP peptide, and quantitative electrophoretic mobility shift assays (EMSA) demonstrated that this interaction stabilizes the complex between the basic-spacer segment and target DNA. Taken together, our results suggest that pX does not enhance bZIP·DNA complex stability by enhancing dimerization or altering the pathway of complex assembly. Instead, the data suggest that pX enhances bZIP·DNA complex stability by aiding the existing monomer pathway. Additional experiments reveal that pX decreases the kinetic specificity of certain bZIP proteins for DNA. To the extent that it is reflected at the transcriptional level, this loss in specificity could have far-reaching consequences for the host cell.

EXPERIMENTAL PROCEDURES

Preparation of bZIP Peptides. A_{71}. The peptide A_{71} contains ATF-2 residues 347–418 and was prepared using pTLSA71 (*54*). The native sequence was modified to make the peptide suitable for fluorescence studies. The pTLSA71 plasmid was engineered from the pLGA65 plasmid (*46*) to incorporate several changes that made the resulting peptide suitable for fluorescence studies. The mutation of leucine 411 to cysteine and cysteine 418 to serine was achieved by

PCR mutagenesis to allow specific covalent modification with fluorophores at the carboxy terminus of the peptide. Site-directed mutagenesis (*55*) was used to convert cysteine 369 to serine to prevent covalent modification within the basic, DNA-binding region.

A_{71} was expressed from pTLSA71 in BL21(DE3) pLysS *Escherichia coli*. The cell pellet was suspended in 10 mL of 10 mM Tris and 100 mM DTT (pH 7.5), lysed by boiling, and clarified by centrifugation. Additional purification resulted from polyethyleneimine precipitation of nucleic acids followed by ammonium sulfate precipitation of A_{71}. A_{71} was purified further by reverse-phase HPLC on a Vydac C_{18} column (10 mm × 250 mm) and characterized by electrospray mass spectrometry (Mass Spectrometry Laboratory, School of Chemical Sciences, University of Illinois at Urbana-Champaign, Urbana, IL) and by amino acid analysis (The HHMI Biopolymer/W. M. Keck Foundation Biotechnology Resource Laboratory, Yale University, New Haven, CT). The predicted (8406.0 Da) and found (8404.6 Da) masses agreed well, and amino acid analysis was consistent with the amino acid content of A_{71}.

$A_{71}{}^{SFLU}$. A_{71} was modified covalently at its unique cysteine with 5-iodoacetamidofluorescein (Molecular Probes) to give $A_{71}{}^{SFLU}$. 5-Iodoacetamidofluorescein (500 μM) was allowed to react with 50 μM A_{71} in 20 mM sodium phosphate (pH 7.4) for 1 h at 25 °C. $A_{71}{}^{SFLU}$ was separated from free fluorescein by one passage through a NAP-10 gel filtration column (Pharmacia) followed by HPLC purification on a Microsorb-MV C18 column (4.6 mm × 250 mm, Rainin). The predicted (8793.0 Da) and found (8792.8 Da) masses for $A_{71}{}^{SFLU}$ agreed well.

$A_{71}{}^{SRHO}$. A_{71} was modified covalently with tetramethylrhodamine-5-iodoacetamide to give $A_{71}{}^{SRHO}$. Tetramethylrhodamine-5-iodoacetamide (350 μM) was reacted with 35 μM A_{71} in 20 mM sodium phosphate (pH 7.4) for 2 h at 25 °C. $A_{71}{}^{SRHO}$ was purified by HPLC on a Microsorb-MV C18 column (4.6 mm × 250 mm, Rainin). The predicted (8793.0 Da) and found (8792.8 Da) masses for $A_{71}{}^{SRHO}$ agreed well. Although our $A_{71}{}^{SRHO}$ sample was contaminated slightly with an oxidized side product, the presence of this impurity had no effect on DNA binding.

A_{32}. A_{32} was prepared by solid-phase synthesis (The HHMI Biopolymer/W. M. Keck Foundation Biotechnology Resource Laboratory) and purified by HPLC on a Vydac C_{18} column (10 mm × 250 mm). The predicted (4290.9 Da) and found (4290.0 Da) masses for A_{32} agreed well, and the results of amino acid analysis were consistent with the amino acid content.

A_{30}. A_{30} was prepared by solid-phase synthesis and modified covalently with 5-iodoacetamidofluorescein to give $A_{30}{}^{SFLU}$. $A_{30}{}^{SFLU}$ was purified by HPLC on a Microsorb-MV C18 column (4.6 mm × 250 mm, Rainin). The predicted (4565.2 Da) and found (4562.6 Da) masses for A_{30} agreed well, and the results of amino acid analysis were consistent with the amino acid content. Peptide concentrations in all cases were determined by amino acid analysis.

JunLZ^{SFLU}. JunLZ^{SFLU} contains Jun residues 285–324 (*56*) followed by one cysteine residue which was covalently modified with fluorescein. JunLZ^{SFLU} was a gift from Jennifer J. Kohler (Department of Chemistry, Yale University).

HBV pX Expression and Purification. pX_{15}, containing HBV pX residues 58–140, was expressed in B834(DE3)

```
          ◄───── basic region ─────►◄spacer◄────── leucine zipper ──────►
A71 MNEDPDEKRRKFLERNRAAASRSRQKRKVWVQSLEKKAEDLSSLNGQLQSEVTLLRNEVAQLKQCLLAHKDS
A32 MNEDPDEKRRKFLERNRAAASRSRQKRKVWVQSGGC
A30 MNEDPDEKRRKFLERNRAAASRSRQKRKVWVQSC
JunLZ                                 RIARLEEKVKTLKAQNSELASTANMLREQVAQLKQKVMNHC
```
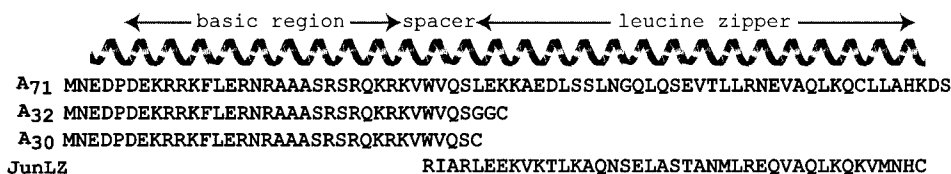
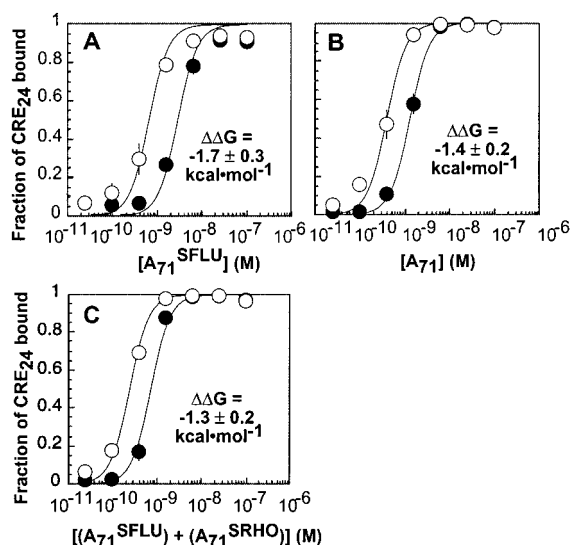FIGURE 2: bZIP peptides used in this study.

FIGURE 3: Influence of pX_{15} and pX on the equilibrium stability of 2:1 bZIP·DNA complexes. (A) Quantitative electrophoretic mobility shift analysis of $(A_{71}^{SFLU})_2$·CRE_{24} complexation in the presence (○) or absence (●) of 10 μM pX_{15} at 25 °C. $K_d(-pX_{15})$ = (8.1 ± 2.4) × 10^{-18} M^2, and $K_d(+pX_{15})$ = (4.2 ± 1.4) × 10^{-19} M^2. (B) Stability of the $(A_{71})_2$·CRE_{24} complex in the presence (○) or absence (●) of 5.8 μM pX at 25 °C. $K_d(-pX)$ = (1.7 ± 0.1) × 10^{-18} M^2, and $K_d(+pX)$ = (1.6 ± 0.3) × 10^{-19} M^2. (C) Stability of the A_{71}^{SFLU}·A_{71}^{SRHO}·CRE_{24} complex in the presence (○) or absence (●) of 5.8 μM pX at 25 °C. $K_d(-pX)$ = (5.4 ± 0.8) × 10^{-19} M^2, and $K_d(+pX)$ = (6.0 ± 0.8) × 10^{-20} M^2. In this case, the ratio of A_{71}^{SFLU} to A_{71}^{SRHO} was held constant at 1:10 to correlate with FRET experiments. Each data point represents the average of at least three independent trials. Error bars represent the standard error.

pLysS *E. coli* from pRMGX15 and purified (46). Full-length HBV pX was expressed in B834(DE3) pLysS *E. coli* from pCRPpX and purified (46). Following purification, pX_{15} and pX were stored dry at −70 °C or dissolved in 0.05% (v/v) aqueous NP-40 and aliquoted into single-use fractions which were also stored at −70 °C. The concentration of pX_{15} used in the experiments varied due to differences in the activity of each preparation; the amount of pX_{15} that was used (between 5 and 20 μM) reflects the amount necessary to reproduce the binding enhancement shown in Figure 3A.

DNA. The DNA duplex CRE_{24} contains the 5′-AGTG-GAGATGACGTCATCTCGTGC-3′ sequence and its complementary strand. The DNA duplex $hsCRE_{24}$ contains the 5′-AGTGGAGATGACAGCTACTCGTGC-3′ sequence and its complementary strand. The preparation, purification, and 5′-end labeling of the oligonucleotides used for this study have been described previously (57).

Electrophoretic Mobility Shift Assays. Binding reactions were performed in binding buffer [137 mM NaCl, 2.7 mM KCl, 4.3 mM Na_2PO_4, 1.4 mM KH_2PO_4 (pH 7.3), 1 mM EDTA, 1 mM DTT, 0.034% (v/v) NP-40, 0.1 mg/mL acetylated BSA, and 10% (v/v) glycerol]. A_{71}, A_{71}^{SFLU}, A_{71}^{SRHO}, or A_{32} was diluted serially from a stock solution

with a known concentration dissolved in PBS buffer. These peptide solutions were incubated with 50 pM [γ-^{32}P]CRE_{24} or -$hsCRE_{24}$ in the presence or absence of pX or pX_{15} for 30 min at 25 °C, allowing the binding reaction to reach equilibrium before it was applied to a running 16 cm × 18 cm nondenaturing 8% polyacrylamide (49:1 acrylamide: bisacrylamide ratio) gel prepared in Tris-glycine buffer (20 mM Tris and 153 mM glycine). Tris-glycine buffer was also used as the electrophoresis running buffer. Samples were loaded and subjected to electrophoresis at 500 V for 30 min at 25 °C. The amounts of complexed and free DNA were quantified on a STORM 840 PhosphorImager (Molecular Dynamics). Equilibrium dissociation constants and free energy values were determined as described previously (58).

Association kinetics experiments also were performed in binding buffer. A_{71} (1 or 2 nM) in the presence or absence of 5 μM pX_{15} was incubated for 30 min at 25 °C in binding buffer. [γ-^{32}P]CRE_{24} (50 pM final concentration) in the presence or absence of $hsCRE_{24}$ (5 nM final concentration) was added to the peptide solution, and aliquots of the reaction mixture were removed and loaded on the gel at varying times. The amounts of complexed and free CRE24 were quantified on a STORM 840 PhosphorImager (Molecular Dynamics). Apparent association rates (k_{app}) were determined by fitting data to the expression $\Theta = c(1 - e^{-k_{app}t})$, where Θ refers to the fraction of DNA bound, c is a constant, and t refers to time (59).

Fluorescence Measurements. Samples used in fluorescence experiments were prepared in binding buffer lacking glycerol and incubated for 30 min at 25 °C before analysis. Equilibrium fluorescence polarization values of solutions containing a range of A_{71}^{SFLU} concentrations in the presence or absence of pX_{15} or pX were measured at 25 °C using an SLM 4800S fluorescence spectrometer (SLM Instruments, Inc.) with an excitation wavelength of 490 nm and an emission wavelength of 520 nm. The measurement reported for each sample was based on an average of 10 successive trials with an average of 10 samplings for each trial. The equilibrium polarization values were fit to provide an equilibrium dissociation constant for dimerization (49). Equilibrium fluorescence polarization values of solutions containing A_{30}^{SFLU} or Jun-LZ^{SFLU} and a range of pX_{15} concentrations were measured at 25 °C using a PTI QuantaMaster C-60 spectrofluorimeter (Photon Technology International) with an excitation wavelength of 490 nm and an emission wavelength of 520 nm. The value reported for each sample was based on an average of polarization values acquired over 30 s. The equilibrium dissociation constant was determined by fitting the data using the method of Benesi and Hildebrand (60, 61). Fluorescence resonance energy transfer experiments with A_{71}^{SFLU} and A_{71}^{SRHO} were performed at 25 °C on a PTI QuantaMaster C-60 spectrofluorimeter with an excitation wavelength of 490 nm, monitoring emission from 500 to 600 nm. The extent of energy transfer was measured as the decrease in fluores-
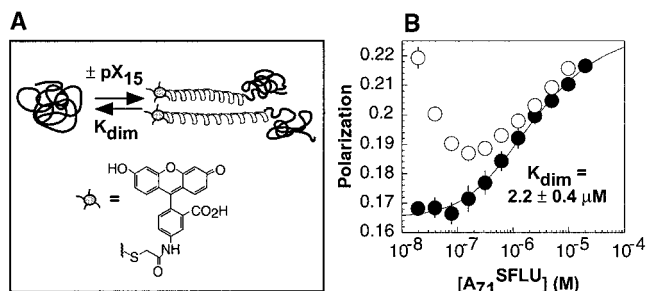
A

B

FIGURE 4: (A) Scheme illustrating the A_{71}^{SFLU} monomer−dimer equilibrium as measured by fluorescence polarization. (B) Fluorescence polarization analysis of the A_{71}^{SFLU} monomer−dimer equilibrium in the presence (○) or absence (●) of 10 μM pX_{15}. Each data point represents the average of at least three independent trials. Error bars represent the standard deviation. $K_{dim}(-pX_{15})$ was determined as described in Experimental Procedures.

cein emission at 520 nm. The equilibrium dissociation constant for dimerization was determined by fitting the data using the method of Benesi and Hildebrand (*60, 61*).

RESULTS

pX_{15} Enhances the Formation of a 2:1 A_{71}^{SFLU}·DNA Complex. Previous work has shown that full-length HBV pX enhances the DNA affinities of a wide range of bZIP peptides and proteins (*45−47*). Initial studies of a truncated version of pX, termed pX_{15}, demonstrated that the potency of pX_{15} as a transcriptional activator in transient transfection assays equals that of full-length pX (*62*). We first set out to establish that pX_{15} also enhances the equilibrium DNA affinities of bZIP peptides, in particular the modified bZIP peptide to be used in our fluorescence studies. Binding isotherms resulting from electrophoretic mobility shift assays (EMSAs) illustrating the affinity of A_{71}^{SFLU} for CRE_{24} in the presence and absence of 10 μM pX_{15} are shown in Figure 3A. pX_{15} supplemented the free energy of the $(A_{71}^{SFLU})_2$·CRE_{24} complex with a $\Delta\Delta G_{obs}$ of -1.7 ± 0.3 kcal mol^{-1}. pX_{15} also increased the stabilities of several other bZIP peptide·DNA complexes (data not shown), in all cases by amounts comparable to those measured with pX (*46*). These results indicate that pX_{15} mirrors pX in its ability to stabilize bZIP·DNA complexes and that the covalent modification of A_{71} with fluorescein does not reduce its ability to interact with pX_{15}. Thus, pX_{15} and A_{71}^{SFLU} are reasonable molecules for assessing the effect of pX on bZIP peptides in solution.

pX_{15} Alters the Fluorescence Polarization of A_{71}^{SFLU}. To determine whether pX_{15} enhances the equilibrium stability of the A_{71}^{SFLU} dimer in solution, we measured the equilibrium dissociation constant of the A_{71}^{SFLU} dimer (K_{dim}) by fluorescence polarization (*63*) as shown in Figure 4A. The polarization of a solution of A_{71}^{SFLU} increased as the peptide concentration increased from 10 nM to 20 μM. A graph of polarization versus the concentration of A_{71}^{SFLU}, shown in Figure 4B, was sigmoidal and was fit to give a K_{dim} of 2.2 $\pm$ 0.4 μM. This value agrees well with the reported value of K_{dim} for ATF-$2_{350−505}$ (*49*). Here, the polarization increased with an increase in peptide concentration, consistent with a transition from a primarily monomeric peptide population at low concentrations to a folded, dimeric population at higher concentrations.

To evaluate whether pX_{15} increases the equilibrium stability of the A_{71}^{SFLU} dimer, we repeated the experiment

described above in the presence of 10 μM pX_{15}. This concentration of pX_{15} was sufficient to increase the affinity of A_{71} for DNA, as seen in Figure 3A. Addition of 10 μM pX_{15} led to little change in polarization at A_{71}^{SFLU} concentrations between 625 nM and 10 μM (Figure 4B). However, addition of 10 μM pX_{15} dramatically increased the polarization of A_{71}^{SFLU} at concentrations of <100 nM. Interestingly, this concentration of pX_{15} also increased the DNA affinity of A_{71} at bZIP concentrations of <100 nM in electrophoretic mobility shift assays (Figure 3A).

While these results indicate that pX_{15} affects the polarization of A_{71}^{SFLU} in solution, the change we observe is not consistent with the prediction that pX_{15} stabilizes bZIP dimers. If pX_{15} were merely to stabilize A_{71}^{SFLU} dimers, one might expect to see a pX_{15}-induced shift of the polarization versus concentration curve toward lower A_{71}^{SFLU} concentrations. Such a shift would reflect a decrease in the equilibrium dissociation constant (K_{dim}) characterizing A_{71}^{SFLU} dimer formation. A simple curve shift is not observed. Rather, the largest pX_{15}-dependent increase in the polarization is observed at the lowest bZIP concentrations, and the pX_{15}-induced polarization change decreases with increasing bZIP concentration (Figure 4B). The observed curve could result from a stabilization of bZIP dimers that is mitigated at high bZIP concentrations by a limiting concentration of active pX_{15}. Alternatively, the curve could result from formation of a monomeric A_{71}^{SFLU}·pX_{15} complex that is incomplete at higher bZIP concentrations due to a limiting amount of pX_{15}. In any case, the polarization results simply indicate that pX_{15} interacts with some form of A_{71}^{SFLU} and emphasize the need for additional experiments to clarify the nature of this interaction.

pX_{15} Does Not Increase Energy Transfer between A_{71}^{SFLU} and A_{71}^{SRHO}. We made use of a different measure of the A_{71} monomer−dimer equilibrium to distinguish between the possible interpretations of the fluorescence polarization experiment. We prepared a pair of A_{71} derivatives labeled at their C-termini with either a donor (A_{71}^{SFLU}) or acceptor (A_{71}^{SRHO}) fluorophore and monitored the monomer−dimer equilibrium by measuring fluorescence resonance energy transfer (FRET) as a function of A_{71}^{SRHO} concentration (Figure 5A). With such an experiment, one expects to see a decrease in donor emission and an increase in acceptor emission as the acceptor concentration increases. As seen in Figure 5B, emission by 50 nM A_{71}^{SFLU} at 520 nm decreased and emission by A_{71}^{SRHO} at 575 nm increased upon addition of 50 nM to 3.2 μM A_{71}^{SRHO}. The change in fluorescein emission at 520 nm as a function of A_{71}^{SRHO} concentration corresponded to an equilibrium dissociation constant for the A_{71} dimer of 0.93 $\pm$ 0.2 μM (Figure 5C). This equilibrium dissociation constant, as determined by FRET, agrees well with the value measured by polarization (K_{dim} = 2.2 $\pm$ 0.4 μM).

Having established that this FRET system is an accurate monitor of the A_{71} monomer−dimer equilibrium, we investigated the impact of pX_{15} on dimerization. If pX_{15} were to increase the equilibrium stability of the A_{71} dimer, one would expect to see an increase in FRET upon addition of pX_{15} to a mixture of A_{71}^{SFLU} and A_{71}^{SRHO} monomers. A mixture of 5 nM A_{71}^{SFLU} and 50 nM A_{71}^{SRHO} (total A_{71} concentration of 55 nM) contains a monomer:dimer ratio of approximately 20:1. Addition of 10 μM pX_{15} to this mixture raised the
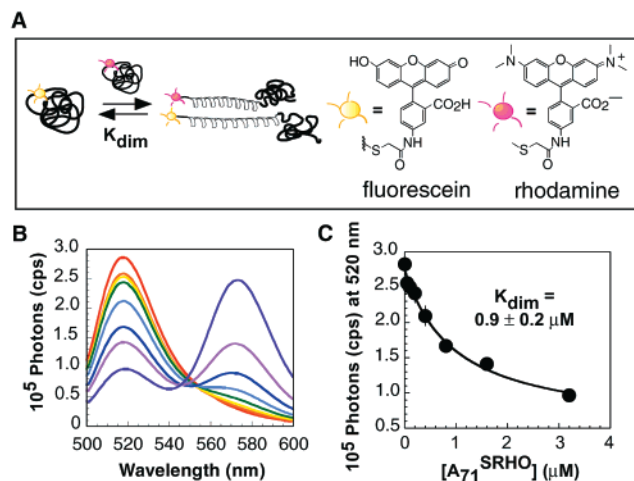
FIGURE 5: Fluorescence resonance energy transfer (FRET) analysis of the A_{71} monomer−dimer equilibrium. (A) Scheme illustrating the A_{71} monomer−dimer equilibrium as measured by FRET. (B) Shown is the fluorescence emission between 500 and 600 nm of 50 nM A_{71}^{SFLU} alone (red) or in the presence of 50 nM A_{71}^{SRHO} (orange), 100 nM A_{71}^{SRHO} (yellow), 200 nM A_{71}^{SRHO} (green), 400 nM A_{71}^{SRHO} (blue), 800 nM A_{71}^{SRHO} (indigo), 1.6 μM A_{71}^{SRHO} (lavender), or 3.2 μM A_{71}^{SRHO} (purple). (C) Determination of the equilibrium dissociation constant (K_{dim}) from the fluorescence emission scans presented in panel B. A graph of the decrease in A_{71}^{SFLU} emission at 520 nm vs the concentration of A_{71}^{SRHO} was fit to give K_{dim} as described in Experimental Procedures. Each data point represents the average of at least three independent trials. Error bars represent the standard error.

baseline of the emission scan slightly but did not lead to the changes associated with FRET, a decrease in emission at 520 nm and an increase in emission at 575 nm (Figure 6A). Addition of pX_{15} to A_{71}^{SFLU} alone also raised the baseline (Figure 6B). By contrast, 10 μM pX_{15} significantly altered the polarization of 55 nM A_{71}^{SFLU} in our initial polarization study (Figure 4B) as well as in polarization experiments using the samples prepared for FRET (Figure 6A, inset). Taken together, these results suggest that pX_{15} binds A_{71}^{SFLU} and alters its polarization, but does not shift the position of the A_{71} monomer−dimer equilibrium.

pX Does Not Increase Energy Transfer between A_{71}^{SFLU} and A_{71}^{SRHO}. We performed an analogous set of experiments using full-length pX. Quantitative EMSA experiments established that pX and pX_{15} cause similar increases in the equilibrium DNA affinity of A_{71} (Figure 3B) and a 1:10 mixture of A_{71}^{SFLU} and A_{71}^{SRHO} (Figure 3C) ($\Delta\Delta G_{obs} = -1.4 \pm 0.2$ kcal mol^{-1} and $\Delta\Delta G_{obs} = -1.3 \pm 0.2$ kcal mol^{-1}, respectively). Spectroscopic experiments revealed that 5.8 μM pX, like pX_{15}, had no effect on the FRET of a mixture of 5 nM A_{71}^{SFLU} and 50 nM A_{71}^{SRHO} (total A_{71} concentration of 55 nM) (Figure 6C). Similar results were observed during experiments including increased concentrations of pX with 55 nM A_{71} (data not shown) or increased concentrations of pX with 550 nM A_{71} (Figure 6D). In each case, addition of pX modestly increased fluorescein emission, whereas a decrease in fluorescein emission (and an increase in rhodamine emission) would be expected were pX to stabilize the A_{71} dimer. Although it did not promote energy transfer, pX also increased the polarization of these samples (Figure 6C, inset).

CRE_{24} Increases the Level of Energy Transfer between A_{71}^{SFLU} and A_{71}^{SRHO}. We performed a control experiment to ensure that a molecule known to stabilize the A_{71} dimer
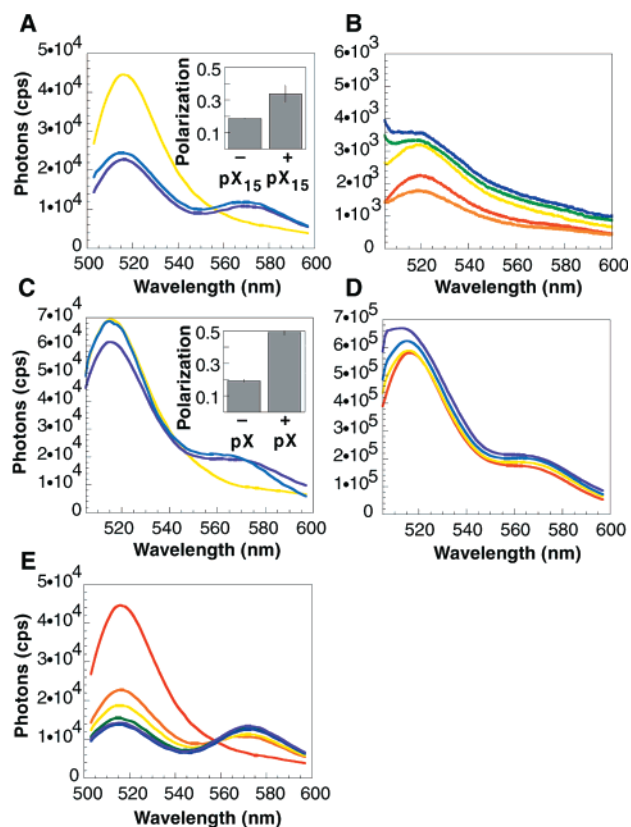

FIGURE 6: Comparison of the effect of pX_{15} and pX and DNA on the equilibrium stability of the A_{71} dimer. (A) FRET analysis of the effect of pX_{15} on the A_{71} monomer−dimer equilibrium. Shown is the fluorescence emission between 500 and 600 nm of 5 nM A_{71}^{SFLU} alone (yellow) or in the presence of 50 nM A_{71}^{SRHO} (purple) or both 50 nM A_{71}^{SRHO} and 10 μM pX_{15} (blue). The inset shows the fluorescence polarization of 5 nM A_{71}^{SFLU} combined with 50 nM A_{71}^{SRHO} in the presence or absence of 10 μM pX_{15}. Each data point represents the average of at least three independent trials. Error bars represent the standard error. (B) Analysis of the effect of pX_{15} on the fluorescence baseline. Shown is the fluorescence emission between 500 and 600 nm of 10 nM A_{71}^{SFLU} alone (red) or with 10 μM pX_{15} (orange), 20 μM pX_{15} (yellow) 40 μM pX_{15} (green), or 60 μM pX_{15} (blue). (C) FRET analysis of the effect of pX on the A_{71} monomer−dimer equilibrium. Shown is the fluorescence emission between 500 and 600 nm of 5 nM A_{71}^{SFLU} alone (yellow) or in the presence of 50 nM A_{71}^{SRHO} (purple) or both 50 nM A_{71}^{SRHO} and 5.8 μM pX (blue). The inset shows the fluorescence polarization of 5 nM A_{71}^{SFLU} combined with 50 nM A_{71}^{SRHO} in the presence or absence of 5.8 μM pX. Each data point represents the average of at least three independent trials. Error bars represent the standard error. (D) FRET analysis of the effect of increased pX concentration on the A_{71} monomer−dimer equilibrium. Shown is the fluorescence emission between 500 and 600 nm of 50 nM A_{71}^{SFLU} with 500 nM A_{71}^{SRHO} alone (red) or in the presence of 2.9 μM pX (yellow), 5.8 μM pX (blue), or 11.6 μM pX (purple). (E) FRET analysis of the effect of CRE_{24} on the A_{71} monomer−dimer equilibrium. Shown is the fluorescence emission between 500 and 600 nm of 5 nM A_{71}^{SFLU} alone (red) or in the presence of 50 nM A_{71}^{SRHO} (orange) with added 6.25 nM CRE_{24} (yellow), 12.5 nM CRE_{24} (green), 25 nM CRE_{24} (blue), or 50 nM CRE_{24} (purple).

increased FRET between A_{71}^{SFLU} and A_{71}^{SRHO}. FRET experiments were carried out under the same conditions described above except that pX_{15} or pX was replaced with the oligonucleotide CRE_{24}. Addition of 6.25−50 nM CRE_{24} to 55 nM A_{71} led to clear and predictable changes in fluorescence emission that were evidence of FRET. Addition of CRE_{24} at concentrations between 6.25 and 25 nM caused
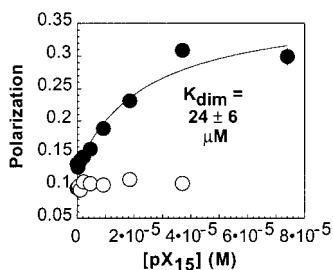
FIGURE 7: Fluorescence polarization analysis of the affinity of pX_{15} for 50 nM A_{30}^{SFLU} (●) or 50 nM $JunLZ^{SFLU}$ (○). Each data point represents the average of at least three independent trials. Error bars represent the standard deviation. The K_d of the $A_{30}^{SFLU} \cdot pX_{15}$ complex was determined as described in Experimental Procedures.

concentration-dependent decreases and increases in fluorescein and rhodamine emission, respectively, as illustrated in Figure 6E. In contrast, addition of CRE_{24} at concentrations >25 nM caused no further change in the emission spectrum. This result is consistent with formation of a 2:1 protein·DNA complex that is complete at 25 nM CRE_{24}. Moreover, addition of pX to a mixture of 5 nM A_{71}^{SFLU} and 50 nM A_{71}^{SRHO} in the presence of between 6.25 and 25 nM CRE_{24} led to a modest increase in emission by fluorescein at 520 nm and a small upward baseline shift near 575 nm (data not shown). With these spectroscopic experiments, we establish that a specific DNA target increases the equilibrium stability of the A_{71} dimer as measured by FRET and that pX does not interfere with FRET within a DNA-bound bZIP dimer. These control experiments strengthen our conclusion that pX does not increase A_{71} dimer stability in the absence of DNA.

pX_{15} Increases Fluorescence Polarization of A_{30}^{SFLU}. The FRET experiments described above suggest that pX does not enhance bZIP dimer formation, yet polarization experiments (as well as previous work) (*36, 45, 47*) suggest that pX binds bZIP peptides and proteins. To further distinguish which portion of the bZIP element interacts with pX_{15}, we investigated the fluorescence polarization behavior of A_{30}^{SFLU} (Figure 2) in the presence and absence of pX_{15}. A_{30}^{SFLU} contains the same basic-spacer region found in A_{71}^{SFLU} but lacks the leucine zipper dimerization region. The fluorescence polarization of 50 nM A_{30}^{SFLU} was measured after incubation with 290 nM to 74 μM pX_{15}. The addition of pX_{15} resulted in a concentration-dependent increase in the polarization of A_{30}^{SFLU} (Figure 7). If it is assumed that the complex possesses a 1:1 stoichiometry, this change corresponds to an equilibrium dissociation constant of 24 ± 6 μM. This experiment indicates that pX_{15} has a significant affinity for the basic-spacer segment of a bZIP protein. We also performed a similar experiment to measure the fluorescence polarization of $JunLZ^{SFLU}$ (Figure 2) in the presence and absence of pX_{15} (Figure 7). $JunLZ^{SFLU}$ contains the zipper region of Jun but lacks the basic region. Therefore, we were able to explore whether pX_{15} has a comparable affinity for any peptide and whether it interacts equally with an isolated zipper segment. Addition of 290 nM to 37 μM pX_{15} to 50 nM $JunLZ^{SFLU}$ caused no significant change in polarization (Figure 7). This result indicates that pX_{15} has a specific affinity for the isolated basic-spacer segment in A_{30}^{SFLU} and little or no affinity for an isolated zipper segment. This result agrees with other work suggesting that pX interacts primarily with the basic segment of the bZIP element (*45–47*).
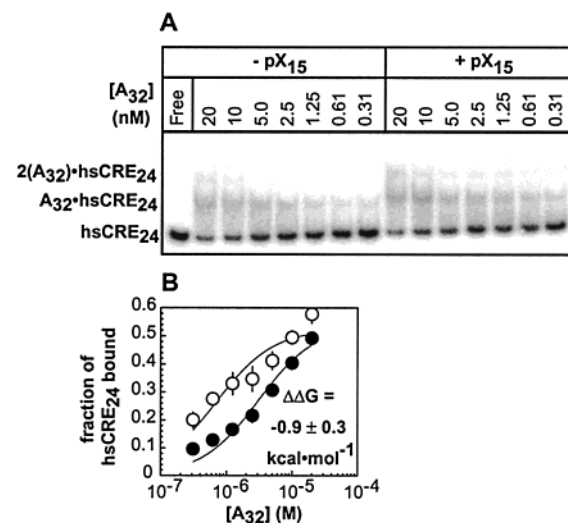

FIGURE 8: Influence of pX_{15} on the equilibrium stability of a bZIP monomer·DNA half-site complex. (A) Gel representative of the equilibrium binding of A_{32} to $hsCRE_{24}$ in the presence (lanes 9–15) and absence (lanes 2–8) of 20 μM pX_{15}. Due to the high peptide concentrations that are necessary to detect monomer binding, it is likely that the second shift that is visible on the gel is due to nonspecific second site binding. (B) Quantitative electrophoretic mobility shift analysis of $A_{32} \cdot hsCRE_{24}$ complexation in the presence (○) or absence (●) of 20 μM pX_{15} at 25 °C. $K_d(-pX_{15}) = (3.1 \pm 0.7) \times 10^{-6}$ M, and $K_d(+pX_{15}) = (7.0 \pm 2.2) \times 10^{-7}$ M.

pX_{15} Enhances Formation of an A_{32}·DNA Complex. To assess whether pX_{15} would stabilize the complex between an isolated basic-spacer region and target DNA, we measured the affinity of A_{32} (Figure 2) for $hsCRE_{24}$ in the presence and absence of 20 μM pX_{15} using EMSA (Figure 8A). pX_{15} supplemented the free energy of the $A_{32} \cdot hsCRE_{24}$ complex by a $\Delta\Delta G_{obs}$ of −0.9 ± 0.3 kcal/mol (Figure 8B). The data suggest that pX_{15} stabilizes both the 1:1 $A_{32} \cdot hsCRE_{24}$ complex and what appears to be a nonspecific higher-order complex. It is not surprising that pX_{15} would act in both of these ways, since prior work has demonstrated that pX enhances both specific and nonspecific DNA binding by bZIP proteins (*36, 45–47*). pX_{15} stabilizes the $A_{32} \cdot hsCRE_{24}$ complex by less than it stabilizes $A_{71} \cdot CRE_{24}$ complexes, suggesting that pX may also enhance the DNA affinity of the second monomer. It is conceivable, therefore, that pX_{15} aids the binding of each bZIP monomer as it assembles on DNA along the monomer pathway.

pX_{15} Alters the Kinetic Specificity of A_{71} Assembly. Since pX_{15} appears to facilitate monomer pathway binding, we asked whether pX_{15} impacts the rate of assembly of the $(A_{71})_2 \cdot CRE_{24}$ complex. Using EMSA, we measured the fraction of CRE_{24} bound by A_{71} as a function of time in the presence and absence of 5 μM pX_{15} (Figure 9A). In the presence of pX_{15}, the association rate was 4 times greater than the rate in the absence of pX_{15}. Thus, the effect of pX_{15} on the equilibrium stability of the $(A_{71})_2 \cdot CRE_{24}$ complex (Figure 3) is due at least in part to an increase in the association rate. We also measured the effect of pX_{15} on the rate with which A_{71} locates a specific CRE_{24} target site in the presence of competing nonspecific DNA (*49*). We found that, in the absence of pX_{15}, the rate of $(A_{71})_2 \cdot CRE_{24}$ complexation was unaffected when a 100-fold excess (5 nM) of nonspecific DNA was added to the binding reaction mixture (Figure 9B). However, when a 100-fold excess of nonspecific DNA was added in the presence of 5 μM pX_{15},
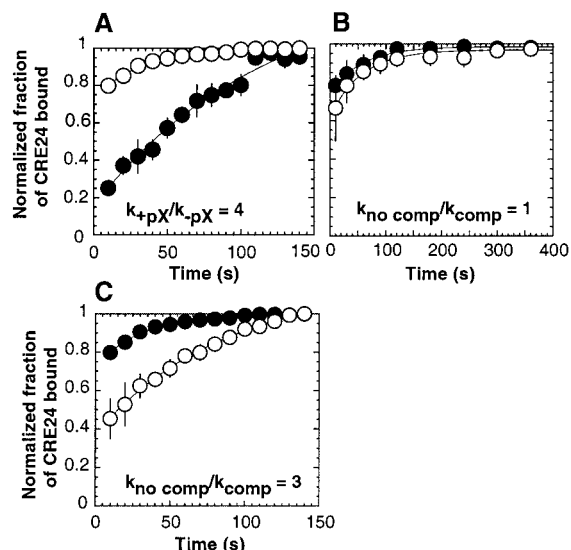
FIGURE 9: Influence of pX_{15} on the rate of $(A_{71})_2$·CRE_{24} complex assembly. (A) The rate of association between 1 nM A_{71} and 50 pM CRE_{24} was measured in the presence (○) or absence (●) of 5 μM pX_{15} using electrophoretic mobility shift analysis at 25 °C. (B) The rate of association between 2 nM A_{71} and 50 pM CRE_{24} was measured in the presence (○) or absence (●) of excess nonspecific DNA (5 nM $hsCRE_{24}$). (C) The rate of association between 1 nM A_{71} with 5 μM pX_{15} and 50 pM CRE_{24} was measured in the presence (○) or absence (●) of excess nonspecific DNA. Each data point represents the average of at least three independent trials. Error bars represent the standard deviation. k_{app} values were determined as described in Experimental Procedures.

the rate of $(A_{71})_2$·CRE_{24} complexation decreased (Figure 9C). These results suggest that the interaction between pX_{15} and A_{71} limits the ability of A_{71} to assembly quickly on a specific DNA target site.

DISCUSSION

A large number of transcription factors, including (but not limited to) the bZIP, bHLHZip, homeodomain (*64*), and Rel/NF-κB (*65*) families, bind DNA to form complexes with a 2:1 protein:DNA stoichiometry. These complexes can assemble along two limiting pathways (Figure 1). The protein can dimerize first and then associate with DNA (the pathway we term the dimer pathway), or it can follow a pathway in which two protein monomers bind DNA sequentially and assemble their dimerization interface while bound to DNA (the monomer pathway). Previous studies have shown that the monomer pathway is followed in the absence of pX by all bZIP and bHLHZip proteins that have been tested (*49–53, 66*) as well as by the Arc repressor (*67*). Here we investigate whether the monomer pathway is still preferred in the presence of pX, or whether pX might promote bZIP dimerization to such an extent that the dimer pathway would become competitive. Our FRET experiments provide a convenient assay for dimer formation in solution and for the ability of other molecules to enhance dimer formation. However, we observe no pX-dependent enhancement in dimer formation. Because dimer formation is the rate-limiting step along the dimer pathway (*49*), we conclude that pX does not promote DNA binding by enhancing the dimer pathway.

Our initial fluorescence polarization experiment with a 71-residue bZIP peptide hinted at a measurable interaction between pX and an isolated bZIP peptide in solution, and

our later experiments localized this interaction to the 30 residues of the basic-spacer segment (Figure 2). This finding agrees with previous work suggesting that the basic-spacer region of a bZIP protein is recognized by pX (*45–47*). Because our FRET experiments indicate that this interaction does not enhance bZIP dimerization, we tested whether it enhances the affinity of a bZIP monomer for DNA containing a target half-site. Using gel mobility shift experiments, we determined that pX increases the stability of the 1:1 complex between a bZIP monomer and DNA. As this complex represents the product of the first step along the monomer pathway (Figure 1), it seems likely that pX increases bZIP·DNA stability by increasing flux along the monomer pathway.

Our conclusion that pX does not enhance bZIP dimer stability agrees with the results of some, but not all, previous work. These prior studies primarily made use of chemical methods to detect changes in the bZIP monomer–dimer equilibrium. An early nonspecific glutaraldehyde cross-linking study revealed no increase in the fraction of bZIP dimers when increasing concentrations of pX were incubated with 9 nM CREB (*45*). However, a more recent nonspecific glutaraldehyde cross-linking study detected a pX-dependent increase in the fraction of GCN4 dimers when pX was incubated with higher bZIP concentrations (>100 nM) (*47*). Since the value of K_{dim} for most bZIP proteins that have been examined falls in the low micromolar concentration range, a bZIP concentration of 9 nM may have been too low to detect a pX-induced shift in the monomer–dimer equilibrium. However, it also must be noted that a glutaraldehyde cross-linking reaction can join two proximal bZIP proteins regardless of whether they are assembled into a properly folded, dimeric structure. pX may exist as a dimer under certain conditions (*47*). Therefore, it is possible that a pX dimer (or higher oligomer) binds a pair of unfolded or partially folded bZIP monomers in such a way that their effective concentration relative to each other is increased. The interaction of each bZIP monomer with pX increases its affinity for DNA and stabilizes the first intermediate along the monomer assembly pathway. The close proximity of the second monomer may in turn facilitate binding of the second monomer and dimer formation on DNA.

The fact that pX does not stabilize bZIP dimers in the absence of DNA sets this transcriptional accessory factor apart from two other proteins that stabilize bZIP·DNA complexes, the viral HTLV-I Tax protein (*68, 69*) and the human bZIP enhancing factor (BEF) (*70*). In both of these cases, it is believed that accessory factor-enhanced dimer formation contributes significantly to the equilibrium stabilization of the bZIP·DNA complex. It is important to note, however, that these conclusions are also based on glutaraldehyde cross-linking studies. By contrast, a recent fluorescence-based study suggests that Tax does not enhance the stability of CREB dimers, and that Tax enhances DNA binding, at least in part, through interactions with the DNA minor groove (*71*). The fact that the results from this fluorescence study also conflict with cross-linking results underscores the need for careful interpretation of these experiments.

Our results also suggest that pX decreases the rate at which a bZIP protein locates a specific target site within the rich cellular environment provided by the nucleus. In the absence

of pX, we believe the monomer pathway is preferred in this environment because it allows a bZIP protein to locate specific DNA more quickly than the dimer pathway (*49*). In the nucleus, the mass action of excess nonspecific DNA favors formation of nonspecific protein·DNA complexes (*72*). While proteins forced to follow the dimer pathway by virtue of a covalent disulfide bond dissociate slowly from these nonspecific protein and DNA competitors, proteins free to bind as monomers do not, and as a result can locate their target sites quickly on specific protein·DNA complexes (*49*). Since pX stabilizes the bZIP monomer·DNA complex, it also might slow dissociation from nonspecific protein and DNA competitors and decrease the rate at which the protein locates a specific DNA sequence. Thus, a pX·bZIP monomer complex may act in a manner that is analogous to that of a covalently linked bZIP dimer, trapping the protein on nonspecific DNA sites. In essence, pX compromises kinetic specificity by offering increased equilibrium stability. It is not difficult to imagine how these effects could favor viral transcription and hamper the accuracy of cellular transcription.

ACKNOWLEDGMENT

REFERENCES

1. Chisari, F. V. (2000) *Am. J. Pathol. 156*, 1118−1132.
2. Feitelson, M. A. (1999) *J. Cell. Physiol. 181*, 188−202.
3. Chen, P. J., and Chen, D. S. (1999) *Semin. Liver Dis. 19*, 253−262.
4. Blumberg, B. S. (1997) *Proc. Natl. Acad. Sci. U.S.A. 94*, 7121−7125.
5. Tiollais, P., Pourcel, C., and Dejean, A. (1985) *Nature 317*, 489−495.
6. Caselmann, W. H. (1996) *Adv. Virus Res. 47*, 253−302.
7. Yen, T. S. B. (1996) *J. Biomed. Sci. 3*, 20−30.
8. Chen, H. S., Kaneko, S., Girones, R., Anderson, R. W., Hornbuckle, W. E., Tennant, B. C., Cote, P. J., Gerin, J. L., Purcell, R. H., and Miller, R. H. (1993) *J. Virol. 67*, 1218−1226.
9. Nakatake, H., Chisaka, O., Yamamoto, S., Matsubara, K., and Koshy, R. (1993) *Virology 195*, 305−314.
10. Zoulim, F., Saputelli, J., and Seeger, C. (1994) *J. Virol. 68*, 2026−2030.
11. Luber, B., Arnold, N., Stürzl, M., Höhne, M., Schirmacher, P., Lauer, U., Weinberg, J., Hofschneider, P. H., and Kekulé, A. S. (1996) *Oncogene 12*, 1597−1608.
12. Yu, D. Y., Moon, H. B., Son, J. K., Jeong, S., Yu, S. L., Yoon, H., Han, Y. M., Lee, C. S., Park, J. S., Lee, C. H., Hyun, B. H., Murakami, S., and Lee, K. K. (1999) *J. Hepatol. 31*, 123−132.
13. Kim, C.-M., Koike, K., Saito, I., Miyamura, T., and Jay, G. (1991) *Nature 351*, 317−320.
14. Andrisani, O. M., and Barnabas, S. (1999) *Int. J. Oncol. 15*, 373−379.
15. Terradillos, O., Billet, O., Renard, C.-A., Levy, R., Molina, T., Briand, P., and Buendia, M. A. (1997) *Oncogene 14*, 395−404.
16. Robinson, W. S. (1994) *Annu. Rev. Med. 45*, 297−323.
17. Murakami, S. (1999) *Intervirology 42*, 81−99.
18. Nomura, T., Lin, Y., Dorjsuren, D., Ohno, S., Yamashita, T., and Murakami, S. (1999) *Biochim. Biophys. Acta 1453*, 330−340.
19. Dandri, M., Petersen, J., Stockert, R. J., Harris, T. M., and Rogler, C. E. (1998) *J. Virol. 72*, 9359−9364.
20. Doria, M., Klein, N., Lucito, R., and Schneider, R. J. (1995) *EMBO J. 14*, 4747−4757.
21. Benn, J., and Schneider, R. J. (1994) *Proc. Natl. Acad. Sci. U.S.A. 91*, 10350−10354.
22. Benn, J., Su, F., Doria, M., and Schneider, R. J. (1996) *J. Virol. 70*, 4978−4985.
23. Chirillo, P., Falco, M., Puri, P. L., Artini, M., Balsano, C., Levrero, M., and Natoli, G. (1996) *J. Virol. 70*, 641−646.
24. Klein, N. P., and Schneider, R. J. (1997) *Mol. Cell. Biol. 17*, 6427−6436.
25. Lee, Y. H., and Yun, Y. (1998) *J. Biol. Chem. 273*, 25510−25515.
26. Prost, S., Ford, J. M., Taylor, C., Doig, J., and Harrison, D. J. (1998) *J. Biol. Chem. 273*, 33327−33332.
27. Chirillo, P., Pagano, S., Natoli, G., Puri, P. L., Burgio, V. L., Balsano, C., and Levrero, M. (1997) *Proc. Natl. Acad. Sci. U.S.A. 94*, 8162−8167.
28. Terradillos, O., Pollicino, T., Lecoeur, H., Tripodi, M., Gougeon, M. L., Tiollais, P., and Buendia, M. A. (1998) *Oncogene 17*, 2115−2123.
29. Su, F., and Schneider, R. J. (1997) *Proc. Natl. Acad. Sci. U.S.A. 94*, 8744−8749.
30. Shintani, Y., Yotsuyanagi, H., Moriya, K., Fujie, H., Tsutsumi, T., Kanegae, Y., Kimura, S., Saito, I., and Koike, K. (1999) *J. Gen. Virol. 80*, 3257−3265.
31. Avantaggiati, M. L., Natoli, G., Balsano, C., Chirillo, P., Artini, M., De Marzio, E., Collepardo, D., and Levrero, M. (1993) *Oncogene 8*, 1567−1574.
32. Mahé, Y., Mukaida, N., Kuno, K., Akiyama, M., Ikeda, N., Matsushima, K., and Murakami, S. (1991) *J. Biol. Chem. 266*, 13759−13763.
33. Faktor, O., and Shaul, Y. (1990) *Oncogene 5*, 867−872.
34. Seto, E., Mitchell, P. J., and Lyen, T. S. B. (1990) *Nature 344*, 72−74.
35. Spandau, D. F., and Lee, C.-H. (1988) *J. Virol. 62*, 427−434.
36. Maguire, H. F., Hoeffler, J. P., and Siddiqui, A. (1991) *Science 252*, 842−844.
37. Qadri, I., Ferrari, M. E., and Siddiqui, A. (1996) *J. Biol. Chem. 271*, 15443−15450.
38. Haviv, I., Shamay, M., Doitsh, G., and Shaul, Y. (1998) *Mol. Cell. Biol. 18*, 1562−1569.
39. Haviv, I., Vaizel, D., and Shaul, Y. (1996) *EMBO J. 15*, 3413−3420.
40. Qadri, I., Maguire, H. F., and Siddiqui, A. (1995) *Proc. Natl. Acad. Sci. U.S.A. 92*, 1003−1007.
41. Hurst, H. C. (1994) *Protein Profile 1*, 123−168.
42. Hurst, H. C. (1995) *Protein Profile 2*, 105−168.
43. Ohno, H., Kaneko, S., Lin, Y., Kobayashi, K., and Murakami, S. (1999) *J. Med. Virol. 58*, 11−18.
44. Barnabas, S., Hai, T. W., and Andrisani, O. M. (1997) *J. Biol. Chem. 272*, 20684−20690.
45. Williams, J. S., and Andrisani, O. M. (1995) *Proc. Natl. Acad. Sci. U.S.A. 92*, 3819−3823.
46. Palmer, C. R., Gegnas, L. D., and Schepartz, A. (1997) *Biochemistry 36*, 15349−15355.
47. Perini, G., Oetjen, E., and Green, M. R. (1999) *J. Biol. Chem. 274*, 13970−13977.
48. Harrison, S. C. (1991) *Nature 353*, 715−719.
49. Kohler, J. J., Metallo, S. J., Schneider, T. L., and Schepartz, A. (1999) *Proc. Natl. Acad. Sci. U.S.A. 96*, 11735−11739.
50. Metallo, S. J., and Schepartz, A. (1997) *Nat. Struct. Biol. 4*, 115−117.
51. Wu, X. L., Spiro, C., Owen, W. G., and McMurray, C. T. (1998) *J. Biol. Chem. 273*, 20820−20827.
52. Park, C., Campbell, J. L., and Goddard, W. A. (1996) *J. Am. Chem. Soc. 118*, 4235−4239.
53. Berger, C., Piubelli, L., Haditsch, U., and Bosshard, H. R. (1998) *FEBS Lett. 425*, 14−18.
54. Hai, T. W,, Liu, F., Coukos, J. W., and Green, M. R. (1989) *Genes Dev. 3*, 2083−2090.
55. Kunkel, T. A., Roberts, J. D., and Zakour, R. A. (1987) *Methods Enzymol. 154*, 367−382.

56. Glover, J. N. M., and Harrison, S. C. (1995) *Nature 373*, 257–261.
57. Metallo, S. J., and Schepartz, A. (1994) *Chem. Biol. 1*, 143–151.
58. Baranger, A. M., Palmer, C. R., Hamm, M. K., Giebler, H. A., Brauweiler, A., Nyborg, J. K., and Schepartz, A. (1995) *Nature 376*, 606–608.
59. Brown, B. M., Bowie, J. U., and Sauer, R. T. (1990) *Biochemistry 29*, 11189–11195.
60. Connors, K. A. (1987) *Binding Constants*, John Wiley & Sons, New York.
61. Benesi, H. A., and Hildebrand, J. H. (1949) *J. Am. Chem. Soc. 71*, 2703–2707.
62. Kumar, V., Jayasuryan, N., and Kumar, R. (1996) *Proc. Natl. Acad. Sci. U.S.A. 93*, 5647–5652.
63. Heyduk, T., Ma, Y., Tang, H., and Ebright, R. H. (1996) *Methods Enzymol. 274*, 492–503.
64. Wolberger, C. (1996) *Curr. Opin. Struct. Biol. 6*, 62–68.
65. May, M. J., and Ghosh, S. (1997) *Semin. Cancer Biol. 8*, 63–73.
66. Wendt, H., Thomas, R. M., and Ellenberger, T. (1998) *J. Biol. Chem. 273*, 5735–5743.
67. Rentzeperis, D., Jonsson, T., and Sauer, R. T. (1999) *Nat. Struct. Biol. 6*, 569–573.
68. Wagner, S., and Green, M. R. (1993) *Science 262*, 395–399.
69. Perini, G., Wagner, S., and Green, M. R. (1995) *Nature 376*, 602–605.
70. Virbasius, C. M. A., Wagner, S., and Green, M. R. (1999) *Mol. Cell 4*, 219–228.
71. Lundblad, J. R., Kwok, R. P. S., Laurance, M. E., Huang, M. S., Richards, J. P., Brennan, R. G., and Goodman, R. H. (1998) *J. Biol. Chem. 273*, 19251–19259.
72. Bray, D., and Lay, S. (1997) *Proc. Natl. Acad. Sci. U.S.A. 94*, 13493–13498.